BRAIN NECROSIS PREDICTION USING A DOSE-LET VOLUME HISTOGRAM (DLVH)

A Thesis
Presented to
The Academic Faculty

By

Justin Yu

In Partial Fulfillment
of the Requirements for the Degree
Master of Science in the
George W. Woodruff School of Mechanical Engineering
Dept of Nuclear & Radiological Engineering and Medical Physics

Georgia Institute of Technology

August 2024

BRAIN NECROSIS PREDICTION USING A DOSE-LET VOLUME HISTOGRAM (DLVH)

Thesis committee:

Dr. CK Chris Wang
Dept of Nuclear & Radiological Engineering and Medical Physics
Georgia Institute of Technology

Dr. Martin Bues
Dept of Radiation Oncology
Mayo Clinic Arizona

Dr. Wei Liu
Dept of Radiation Oncology
Mayo Clinic Arizona

Dr. Stella Flampouri
Dept of Radiation Oncology
Emory University

Date approved: 5/13/24

For my best friend: Kara Gieseking

飛べ

TABLE OF CONTENTS

LIST OF TABLES

LIST OF FIGURES

LIST OF ACRONYMS

AE Adverse Event

BN Brain Necrosis

CCC Concordance Correlation Coefficient

CNS Central Nervous System

CTV Clinical Target Volume

DLVC Dose-LET Volume Constraint

DLVH Dose-LET Volume Histogram

LET Linear Energy Transfer

MC Monte Carlo

MRI Magnetic Resonance Imaging

NTCP Normal Tissue Complication Probability

PT Proton Therapy

PTV Planning Target Volume

RBE Relative Biological Effectiveness

RN Radionecrosis

SUMMARY

Purpose: A novel tool of dose linear-energy-transfer (LET) volume histogram (DLVH) was utilized to derive dose-LET volume constraints (DLVCs) for brain necrosis (BN) in central nervous system (CNS) cancer patients treated with proton therapy by comparing DLVHs between the control group and adverse event (AE) group.

Methods: A retrospective analysis of an institutional outcomes database was performed to find adult CNS cancer patients undergoing proton therapy who developed BN after treatment, forming the AE group. Patients who did not develop BN post-treatment were matched and paired with the AE patients by radiation dose, fractionation, tumor stage, and BN grade. Dose and LET distributions were calculated by an in-house developed Monte Carlo dose engine, which were used to construct DLVHs of the brain for all patients. The DLVH indices, $V(d\ \text{Gy}, l\ \text{keV}/\mu\text{m})$, which measures the percentage of the volume in the selected structure that has a dose at least d Gy and a LET at least l keV/μm, were compared in the dose-LET plane between the control and AE group and a p-value map in the dose-LET plane was then derived using the Mann-Whitney U Test. DLVCs were then derived from statistical significant features found in the p-value map to differentiate the control and AE group. Reproducibility was evaluated by calculating the concordance correlation coefficient (CCC) voxel-wise throughout the examined dose-LET space.

Results: 17 patients were analyzed; 7 AE patients matched to 10 control patients. Two DLVCs were derived from these regions: DLVC1 is $V(56.5\text{Gy}, 0\text{keV}/\mu\text{m})$, representing a high dose constraint (p=0.047), and DLVC2 is $V(43.5\text{Gy}, 4.25\text{keV}/\mu\text{m})$, representing a high LET constraint (p=0.039).

Conclusion: DLVH was successfully used to deduce DLVCs for CNS cancer patients undergoing proton therapy. The derived DLVCs can be used in the proton therapy plan evaluation retrospectively and in the treatment planning prospectively to reduce possible BNs. This study demonstrates evidence of the LET-enhancing effect for the AE initialization in proton therapy.

CHAPTER 1
INTRODUCTION AND BACKGROUND

1.1 Background

Radiation therapy (RT) is a mainstay of cancer treatment, with photons and electrons comprising the two main types of external beam radiation delivered to patients undergoing RT. In the past few decades, however, particle therapy has become increasingly utilized and sophisticated with a rapid pace of technical development. Particle therapy includes proton therapy (PT), the focus of this study, but heavier charged particles such as carbon also fall under its umbrella.

The reason for particle therapy's attractiveness as a treatment modality arises from the physics of charged particles' interactions with matter. As shown in Figure 1.1, the Bragg peak exhibited by charged particles is responsible for the sharp drop in radiation dose to downstream organs at risk (OARs), in contrast to photon exit doses which are much more gradual [3]. The sharp drop-off of the Bragg peak gives rise to the superior dose conformity to the targets compared to photon therapy and is one of the main drivers behind continued research and development in particle therapy.

Despite this, radiation induced adverse events (AEs) still occur in patients undergoing particle therapy [1]. AEs and their accompanying side effects can range from minor nuisances requiring no intervention to debilitating and painful. Side-effects of radiotherapy are estimated to cause thousands of dollars of additional financial cost on patients for the management of side effects, as well as the additional burden created on medical resources and personnel to provide necessary care [2]. Therefore, it is highly worthwhile to develop methods of predicting and avoiding side-effects in RT.

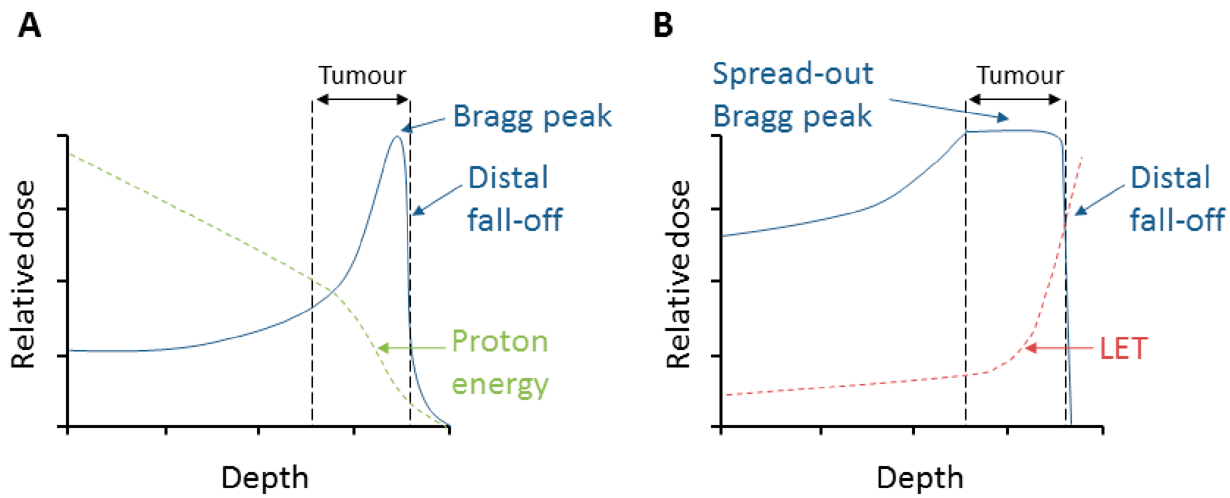

Figure 1.1: Diagram of the Bragg peak (left) and spread-out Bragg peak (SOBP) (right). Figure from Vitti, et al. [3].

1.2 Proton Therapy Physics

Protons are a direct ionizing radiation, who primarily interact with matter through multiple Coulomb interactions with atomic outer layer electrons. When passing through a medium such as water or tissue, a proton loses kinetic energy along its way in a continuous manner. The average rate of energy loss of protons, the stopping power *S*, is mathematically expressed:

$$S = -\frac{dE}{dx} \tag{1.1}$$

where E is the energy of the proton, and x is the distance of travel of the proton [4]. Equation 1.1 describes the energy deposited from the proton to the medium per unit distance. The other often used term of stopping power is linear energy transfer (LET). As protons lose kinetic energy to the environment, the LET increases monotonically along the direction that protons penetrate [5]. The same physical dose deposited by the high-LET protons in a tissue situated in the distal end of the spread-out Bragg peak (SOBP) may have different biological effect (i.e. cell kill) compared to dose from the conventional low-LET photon radiation. The ratio between the two is referred to as relative biological effectiveness (RBE).

The LET of protons, as mentioned, is the highest at the end of the proton's range, which is likely

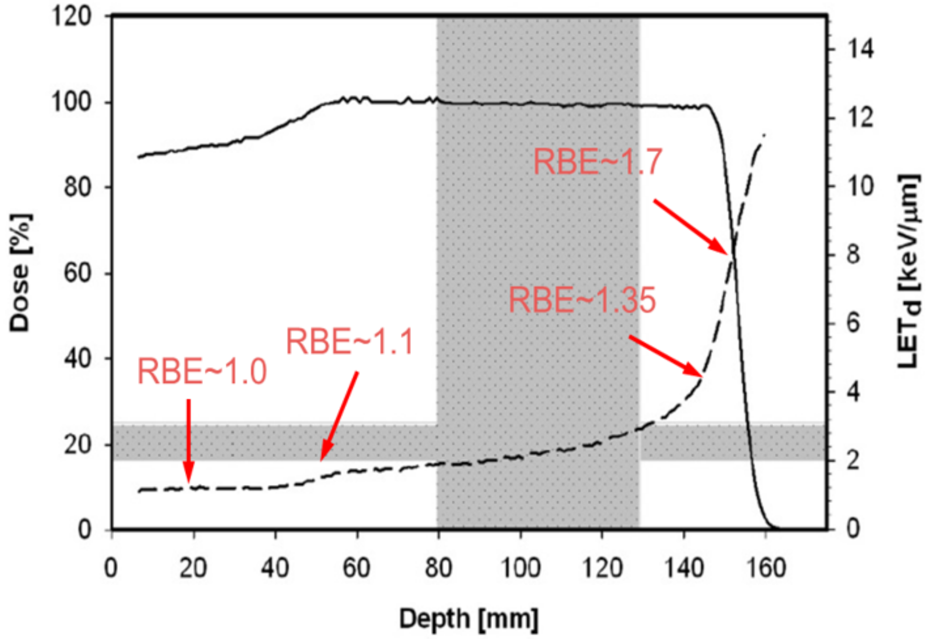

Figure 1.2: RBE variation along the length of a spread-out Bragg peak (shaded region). Note the correlation of RBE and LET (dotted line). Figure from Paganetti, et al. [5].

to abut distal OARs. Currently available treatment planning software fixes the RBE of protons at a constant value of 1.1 for clinical PT plans. However, this assumption of a constant RBE does not incorporate LET, only physical dose, and individual attempts at modeling RBE oftentimes do not agree with other RBE models. The proton RBE close to the end of its range can be as high as 1.7 as illustrated in Figure 1.2. The current, incomplete understanding of these complex radiobiological processes may lead to sub-optimal tumor control and/or adverse events for patients [6, 7]. The precise effect of LET on RBE, and ultimately patient outcomes, is currently a hotly debated topic in the field of proton therapy. Therefore, LET is a highly valuable target to better control for predicting and mitigating radiation-induced AEs.

1.3 Adverse Events in Proton Therapy

Necrosis events resulting from proton therapy has been previously studied by many different groups. According to Indelicato et al, the proposed mechanism for CNS necrosis formation with the most evidence is vascular endothelial damage leading to oligodendrocyte damage and demyelination [8]. Based on this reasoning, the greater ionization density due to the higher LET at the distal end of the Bragg peak will lead to greater cell damage and therefore greater risk of AEs such as necrosis. There are several published studies supporting this hypothesis. In Grosshans et al, 14 pediatric ependymoma patients receiving PT developed MRI imaging changes post-treatment. The dose and LET distributions for these patients were recalculated in a MC engine for analysis. "It was found that higher LET values, not only dose, were associated with damage to normal brain parenchyma", according to the authors [9].

In Fossum et al., an analysis of 11 H&N patients undergoing proton therapy discovered that when comparing the physical model (RBE = 1.1) and biological model (RBE = $(1.1)[0.08(LET_d) + 0.88]$) of the dose distributions, all patients had elevated biological dose than physical dose [10]. Two of the eleven patients exhibited adverse events (one mucosal ulceration, one osteoradionecrosis), and both AE locations coincided with biological hotspots. The authors conclude that "increases in dose predicted by the biological model are clinically relevant and that LET and RBE corrections and optimization should be a component of the treatment-planning process in proton therapy".

In contrast, Garbacz et al. similarly found a slight elevation of LET_d in necrotic voxels compared to dose-matched control voxels for 45 patients receiving treatment for skull base tumors. However, the analysis of the LET_d in normal voxels showed very high intra-patient heterogeneity. Because the analysis was done voxel-wise, the authors concluded that "single-voxel LET_d was not sufficient for prediction of necrosis and that further aspects, as for instance the spatial distribution of LET_d in brain structures, might have played a role" [11]. This is an example of the fact that there is not a universal consensus on the LET effect on CNS necrosis. Some investigators reported the evidence for the LET effect to be weak or not-significant [12–14]. This underlines the need for more data and research into this topic so that consensus can be reached among physicists and clinicians overseeing treatments for their patients.

1.4 LET Optimization in Proton Therapy

Despite the debate on the exact nature of the LET effect on proton therapy, LET optimization is a highly active area of research. Paganetti et al. states, "LET based optimization techniques should be implemented clinically as they allow judging treatment plans based on dosimetric indices while likely reducing the risk for normal tissue toxicities" [15]. However, the topic of LET optimization is complex, with many competing frameworks and models existing simultaneously [16].

An early success in LET optimization was published by Liu et al; the investigators optimized the plans for 14 H&N proton patients with LET distribution as one of the primary weighting factors and introduced both setup and range uncertainties to evaluate the robustness of LET optimization [17]. The objective function of the optimization algorithm was set up to explicitly maximize LET in the CTV and minimize it in OARs. With minimal perturbations to physical dose distribution and plan robustness, LET was significantly reduced in the cord, brain stem, and oral cavity compared to a non-LET optimizing algorithm. This successfully demonstrated that with the right optimization objectives, clinical plans can be improved upon with respect to LET distribution without sacrificing robustness or dose coverage. The optimization algorithm was also applied to prostate, lung, and new H&N proton plans, with similar success in reducing LET in OARs, demonstrating the versatility of this method [18]. Other papers on LET optimization strategies have been published regarding reducing hotspots in base of skull tumor plans [19], and most recently proton FLASH cases [20, 21].

Taken together, these studies demonstrate that LET optimization leads to better therapeutic results as well as lower incidences of adverse events for proton therapy patients. One obstacle to greater consideration of LET during treatment planning is the lack of an easy and intuitive visualization of both dose and LET information in currently available treatment planning systems (TPS). While dose volume histograms (DVH) are used ubiquitously in treatment planning, LET information is entirely absent, even though the role of LET in tumor control and side effects is extremely important. Therefore, a new tool is needed to combine dose and LET in a single graphical plot.

1.5 Dose-LET Volume Histogram Studies

The Dose-LET Volume Histogram (DLVH) is a novel method to incorporate LET information into the DVH [22]. Given that proton therapy plans are calculated with Monte Carlo (MC) methods so that both dose and LET are known for each voxel [23–27], the DLVH adds a second dimension of LET to the DVH, creating a dose-LET plane that all voxels will map to. With this, DLVH indices can be calculated for the structure being analyzed, where V(d Gy, l keV/μm) is the number of voxels that has dose of at least d Gy LET of at least l keV/μm, normalized to the total number of voxels in the contour. Isovolume lines can be added to the DLVH to better visualize important features and thresholds in the space.

Using the DLVH method, researchers have been able to characterize the LET effect for various adverse effects for proton therapy patients. Prostate cancer patients undergoing PT who developed the adverse event of rectal bleeding were analyzed [22, 28]. With the DLVH, the LET distribution was found to be significantly different between the rectal bleeding cohort and the control cohort, as illustrated in Figure 1.3. Two dose-LET volume constraints (DLVCs) were identified; a high dose constraint and a high LET constraint. The two DLVCs were found to be statistically significantly different for the high dose constraint (p = 0.010) and the high LET constraint (p = 0.007). Using the DLVH method, the authors were able to demonstrate both the LET effect on the development of side effects in PT.

In another example, the same DLVH method was used by Yang, et al (2022) to characterize outcomes differences for patients who were treated with VMAT or PT for head and neck cancers and developed mandible osteoradionecrosis (ORN) [29]. The LET information also assisted with getting an empirical estimate of the RBE for mandible ORN, showing significant departure from the constant 1.1 value of RBE assumed for typical treatment planning purposes in PT. Similar to the prostate case, DLVCs can be derived from the DLVH information to better guide treatment planning for future patients.

Most recently, the DLVH method was used to characterize all adverse events (CTCAEv4.0

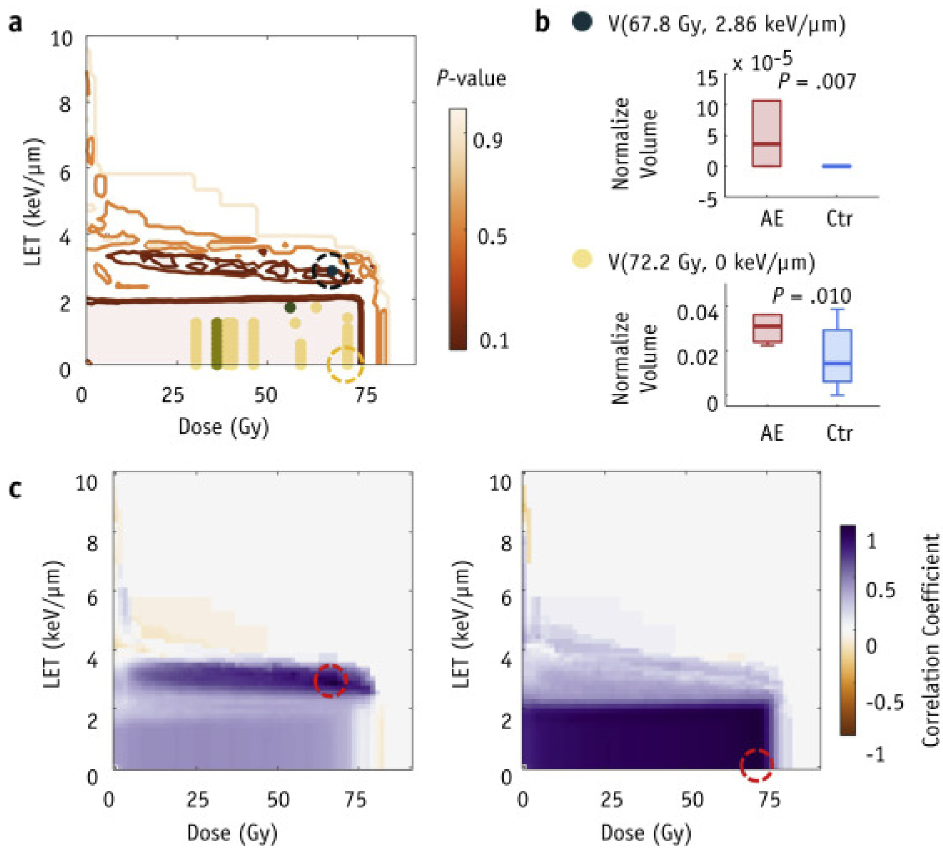

Figure 1.3: Significant differences were found in the treatment plans of rectal bleeding patients vs normal patients using the DLVH. Figure from Yang et al (2021). [22]

grade $\geq$ 3) experienced by a cohort of patients undergoing PT for head and neck cancers [30]. This is shown in Figure 1.5. Of 20 AE patients (out of 113 total patients), 13 of the patients had the region exhibiting the side effects contoured carefully by the experienced treating radiation oncologists facilitated by follow-up surveillance imaging studies. A notable result of having the contoured AE region allowed for the spatial distribution of AE voxels compared with the spatial distribution of high dose or high LET voxels in the same region. The clusters of AE voxels were found to oftentimes be outside of the primary treatment volumes for the out-of-field AEs, and the dose-LET product (xBD) was found to be a strong descriptive feature to predict where AE initialization occurs (i.e. the dosimetric seed spots). This further illustrates the complexity of the LET effect on biological outcomes for proton therapy and highlights the need for additional research in the topic.

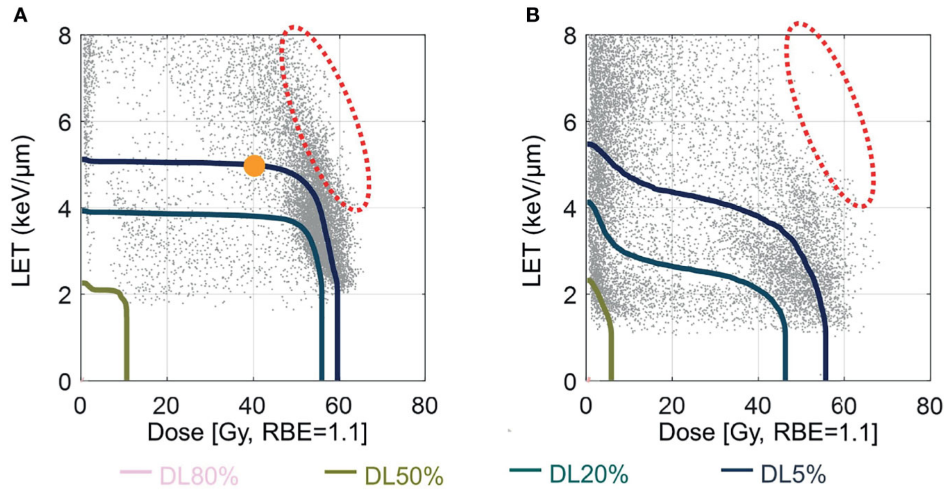

Figure 1.4: DLVH of a patient that developed ORN (left) and didn't develop ORN (right). It can be seen that there is a much lower proportion of voxels in the high LET region (dotted oval) in the normal patient. Figure from Yang et al (2022). [29]

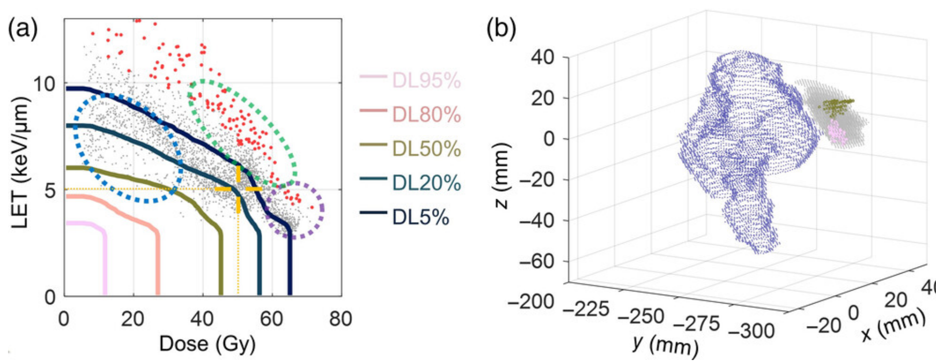

Figure 1.5: Voxels of AE seed spots for a patient experiencing ORN (right) compared to the DLVH (left). The seed spots were selected by grouping the voxels with the highest 5% of dose and LET from the DLVH. Figure from Yang et al (2022). [30]

Taken together, these publications demonstrate 1) the value and the versatility of the DLVH method for evaluating PT treatment plans and characterizing adverse events for cancer patients treated with proton therapy and 2) the repeated demonstration of the synergistic effects of both dose and LET in AE initialization in different disease sites. This makes the DLVH a very attractive tool to continue to investigate the LET-enhancing effect and its influence on adverse events in proton therapy.

1.6 Project Aims

The purpose of this project is to extend the previously described DLVH method to predicting specifically brain radionecrosis (RN) in CNS cancer patients treated with proton therapy. By comparing DLVHs between the AE group and control group, dose-LET volume constraints (DLVCs) will be derived and DLVCs can be used to characterize the possible incidence of brain RN in CNS cancer patients treated with PT.

CHAPTER 2
METHODS

2.1 Patient Selection

All patients in this study were treated at the proton therapy center of the author's home institution; the proton delivery system for all analyzed patients was a Hitachi PROBEAT-V system. An institutional database of radiation therapy patients' outcomes following treatment was searched for CNS cancer patients treated with PT, who have noted incidences of brain radionecrosis (BN) (CTCAE Grade ≥ 1). The BN was identified in these patients in post-treatment surveillance MRI scans by the interpreting radiologist. The scans of the patients with suspected BN were then reviewed by a radiation oncologist and the diagnosis of BN confirmed or rejected. Patients with confirmed BN are henceforth formed as the adverse events (AE) group.

The AE group was further filtered by excluding all patients that were under 18 years old at the time of treatment, had received prior RT, had received boost doses in their treatment plan, had hypofractionated treatment schedules (Gy/fx $>$3Gy), and had not completed their full treatment course (e.g. patient deceased before treatment completion). The institutional patient outcomes database post-treatment was searched again for control patients that did not experience radionecrosis and matched the prescription dose, number of fractions, and met the same inclusion criteria of the AE group.

Potential control patients with the same dose and fractionation as AE group patients were further filtered down by matching primary tumor stage, smoking status, and chemotherapy status. The control patients and AE patients' electronic medical records in Epic (Madison, WI, USA) were searched for this data, and patients that had missing information were excluded from analysis. Finally, control patients were matched with AE patients whose tumor stage, smoking and chemo status were identical to their own. For some AE patients, two control patients were matched based on these criteria to increase the statistical power of the analysis.

2.2 DLVH analysis

All patients, control and AE, were treated with proton plans that had the dose and LET calculated by an in-house Monte Carlo (MC) proton dose and LET calculation engine. Details on the MC software can be found in Deng, et al and related publications [23–27]. The MC-derived dose and LET maps of the treatment plans, as well as the RT structure sets of the selected patients were exported from our commercial treatment planning system (Eclipse ver. 15.6). These DICOM files were processed in MATLAB to generate the DLVHs of the brain for each patient.

DLVH generation and data analysis follows the methods described in Yang, et al (2021) [22]. To summarize, the dose and LET of each voxel in the selected contour are plotted on a 2D graph with dose on the x-axis and LET on the y-axis. The DLVH index at each combination of dose and LET is calculated as the fractional volume of the contoured structure that has a dose of at least d Gy and an LET of at least $l$keV/μm. From the DLVH index, iso-volume lines can be drawn in the DLVH for easier visualization.

DLVH data was binned into 102 bins each in the dose direction and the LET direction, yielding a total of 10,404 dose-LET combinations. The DLVH index as previously defined was found for each patient at each dose-LET combination in the DLVH. For each combination, the Mann-Whitney U test was performed on the collective DLVH indices $V(d,l)$ of the AE group vs the control group, and the resulting *p*-values *p(d,l)* were plotted in the dose-LET plane to create a *p*-value map. By comparing the DLVHs between the AE group and control group voxel-wise using the Mann-Whitney U test, the derived *p*-values map shows where there were significant differences between the AE group and the control group in the dose-LET space. A map of the concordance correlation coefficient [31] was also calculated to evaluate the reproducibility of the data.

Dose-LET volume constraints (DLVC) were derived from the observed typical features to differentiate between the AE group and the control group based on the *p*-value map. The features used to guide DLVC selection include the absolute *p*-values, the relative *p*-values (i.e. local minima), and the actual dose/LET values corresponding to these points of interest. For every DLVC, the corresponding DLVH index, *V(d,l)*, was calculated for each patient and compared between the AE group and control group.

CHAPTER 3

RESULTS

3.1 Patient Cohort

In total, 7 radionecrosis patients met all inclusion criteria and were paired with 10 control patients for a total of 17 patients to derive DLVHs from. The patient data is summarized in Table 3.1. AE Patient A was paired with Patients B and C for analysis purposes, and similarly AE Patients D and I had two control patients each. Total delivered dose ranged from 54 to 76 Gy for all patients.

Table 3.1: Summary of patient treatment data.

Patient	Necrosis	RN Grade	Dose (cGy)	# of Fractions	Primary Tumor Stage
A	Yes	2	5400	30	3
B	No	n/a	5400	30	3
C	No	n/a	5400	30	3
D	Yes	2	5400	30	3
E	No	n/a	5400	30	3
F	No	n/a	5400	30	3
G	Yes	2	5404	28	2
H	No	n/a	5404	28	2
I	Yes	1	7500	30	4
J	No	n/a	7500	30	4
K	No	n/a	7500	30	4
L	Yes	1	7600	30	4
M	No	n/a	7600	30	4
N	Yes	1	5400	30	1
O	No	n/a	5400	30	1
P	Yes	1	5400	30	2
Q	No	n/a	5400	30	2

DLVHs of the brain were successfully derived for all patients. An example of the DLVHs from a control-AE patient pair is shown in Figure 3.1. In the normal patient's DLVH, the high LET region (>4 keV/μm) is less densely populated than the AE patient's DLVH, while the prescription dose was identical between the two patients. The isovolume line being more pushed out from the origin supports the observation that a greater percentage of voxels have high LET in the AE patient's brain contour than the control patient's.

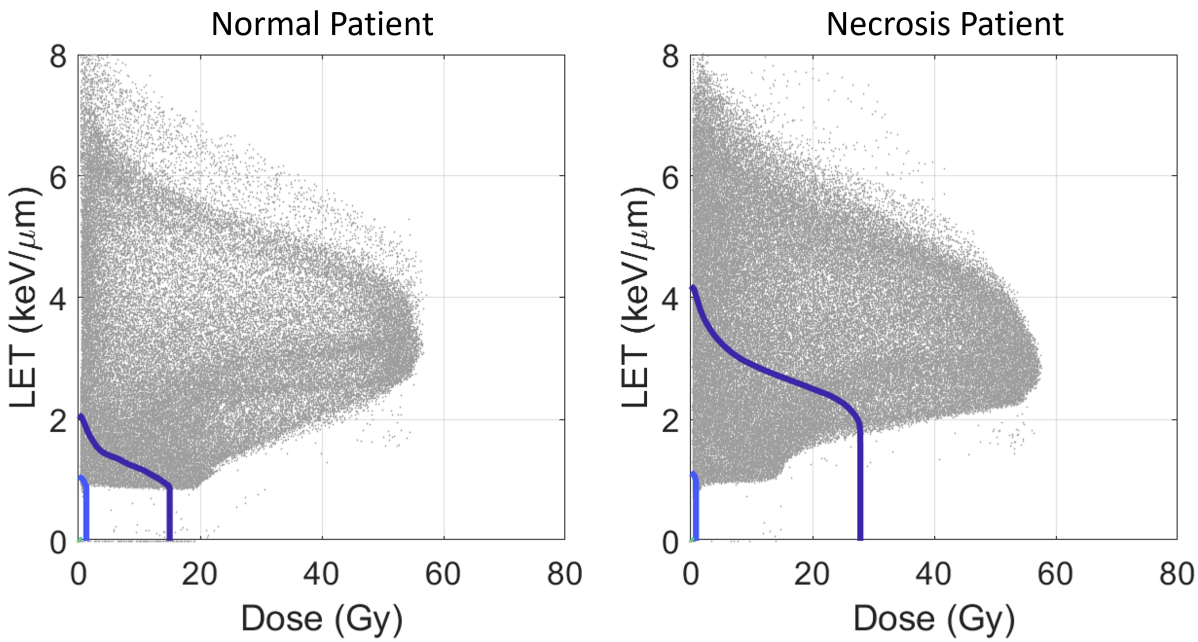

Figure 3.1: An example of two DLVHs, one from a control patient (L) and the other one from its paired AE patient (R). The two colored lines over the DLVH are iso-volume lines indicating two percentile volumes (20% and 5% for light and dark blue respectively).

3.2 DLVH Analysis

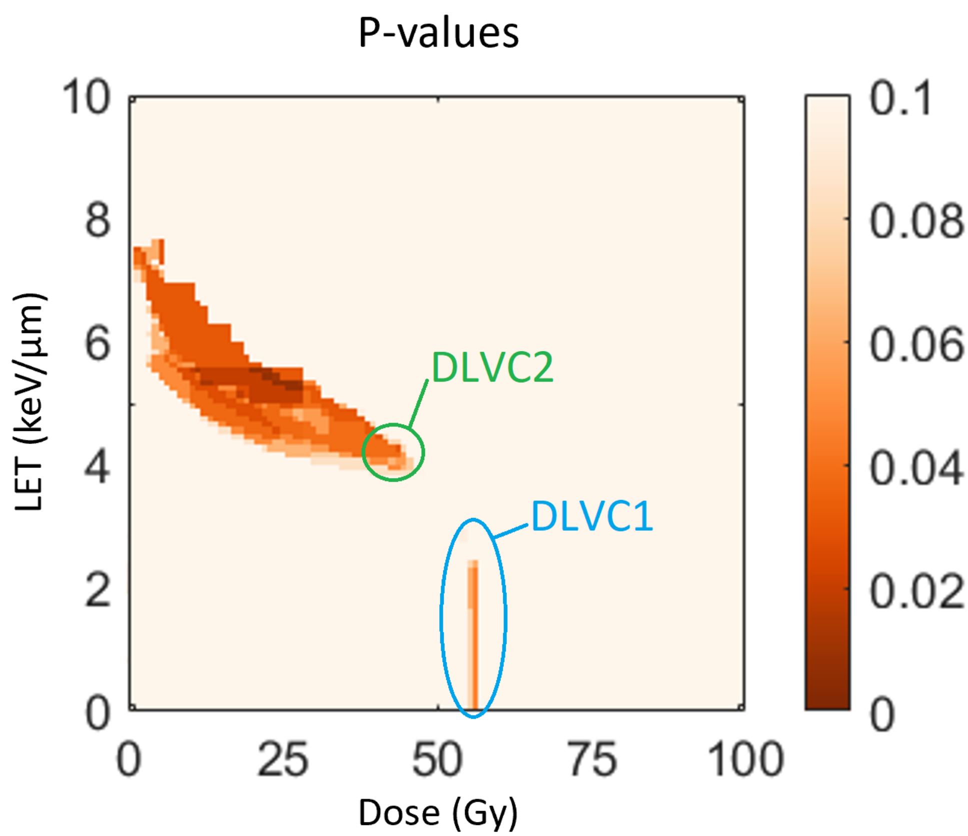

Figure 3.2: DLVH *p*-values map. Darker colors indicate lower *p*-values. DLVCs derived by the circled features in the map.

In Figure 3.2, two distinct areas of statistically significant difference can be observed, highlighted in blue and green. These regions of statistically significant difference between the AE group and control group indicate features to differentiate the AE group from the control group, among which dose-LET volume constraints (DLVCs) can be derived. The first region, the thin line around 56Gy with low LET, corresponds to a high-dose constraint, DLVC1, which could be derived by selecting the position with a local minimum of the *p*-value in this region; this yielded a constraint of D = 56.5Gy for the LET range of 0-2.5 keV/μm.

The second region is the island with a dose spanning from 0Gy<D<44Gy and an LET ranging from 4-8keV/μm, corresponding to a high-LET constraint, DLVC2, which was chosen from the rightmost point of the island in Figure 3.2, facilitied by clinical insights that RBE cannot be larger than 1.7 based on previously published literature, yielding a constraint of D = 43.5Gy and LET = 4.25 keV/μm. The two DLVCs are summarized in Table 3.2.

Table 3.2: Summary of derived DLVC thresholds.

Constraint	Dose (Gy)	LET(keV/μm)
DLVC1	56.5	0
DLVC2	43.5	4.25

3.3 Comparison of DLVH index: *V(d,l)* between the AE and control patients

At each DLVC, the corresponding DLVH index, *V(d,l)*, i.e. the fractional volume of the brain with a dose of at least *d* Gy and an LET of at least *l* keV/μm was calculated for each patient. For example, 0.606% of the brain volume in Patient A received a dose of 56.5Gy or higher and an LET of at least 0 keV/μm (constraint 1), and 0.134% of the brain volume of Patient A received a dose of at least 43.5Gy and an LET of at least 4.25 keV/μm. The results are summarized in Table 3.3.

Table 3.3: DLVH index: *V(d,l)* at each DLVC for every patient.

Patient	Necrosis	RN Grade	V_{DLVC1}%	V_{DLVC2} %
A	Yes	2	0.00%	0.05%
B	No	NA	0.00%	0.002%
C	No	NA	0.00%	0.005%
D	Yes	2	0.05%	0.013%
E	No	NA	0.00%	0.002%
F	No	NA	0.00%	0.000%
G	Yes	2	0.00%	0.026%
H	No	NA	0.00%	0.001%
I	Yes	1	8.21%	0.000%
J	No	NA	7.45%	0.003%
K	No	NA	4.71%	0.000%
L	Yes	1	7.40%	0.000%
M	No	NA	6.09%	0.001%
N	Yes	1	0.00%	0.045%
O	No	NA	0.00%	0.034%
P	Yes	1	0.00%	0.000%
Q	No	NA	0.00%	0.000%

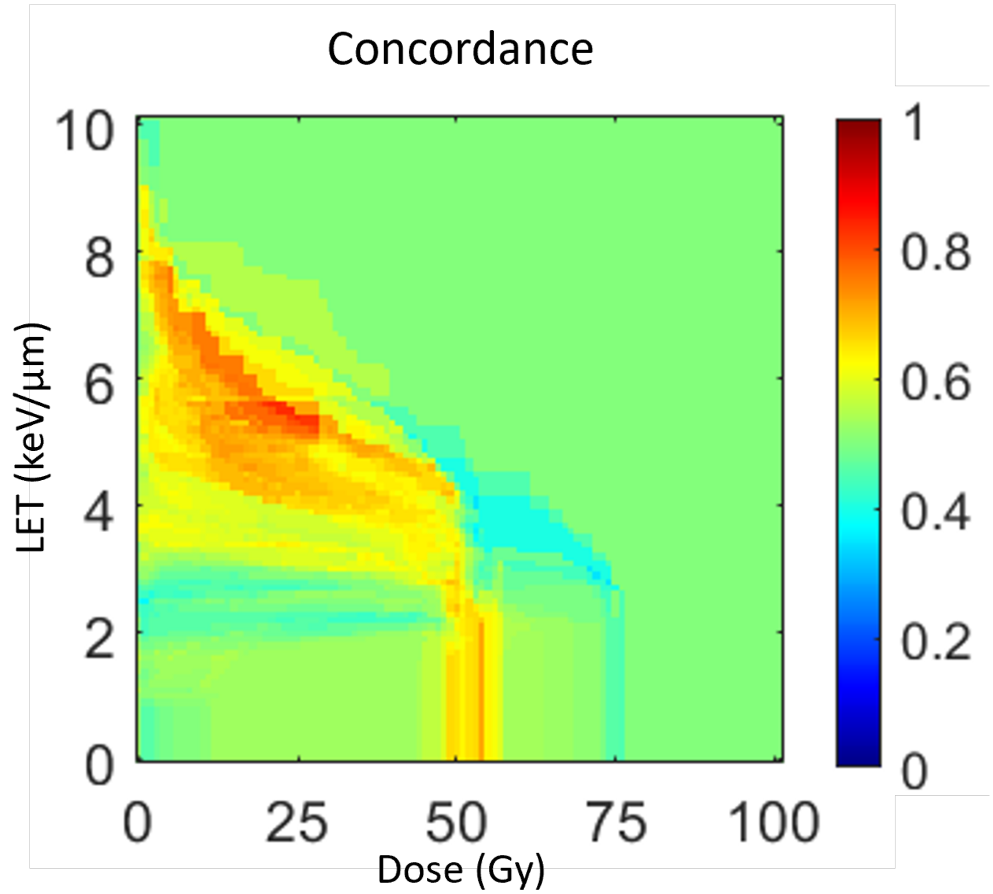

Figure 3.3: Concordance correlation coefficient map showing high reproducibility in voxels with p<0.05.

The concordance map of the *p*-values was shown in Figure 3.3. It shows high concordance ($\geq$0.7) in the regions where DLVC 1 and 2 are derived from, indicating that the DLVH index difference between the control and AE groups is highly reproducible. This approach has been successfully utilized in previous medical image analysis, for example in fMRI data analysis [32].

The data from Table 3.3 was plotted with a box and whisker plot in Figure 3.4. It was observed that the AE patients experienced a higher average DLVH index than the control patients for both DLVC 1 and 2. The absolute difference in mean DLVH index between AE and control patients was greater for the high dose constraint (DLVC1), with 2.39% of voxels in necrosis patients exceeding 56.5Gy vs 1.83% of control patient voxels (p=0.047). For DLVC2, the difference was 0.02% vs 0.00% between AE and control patients (p=0.039).

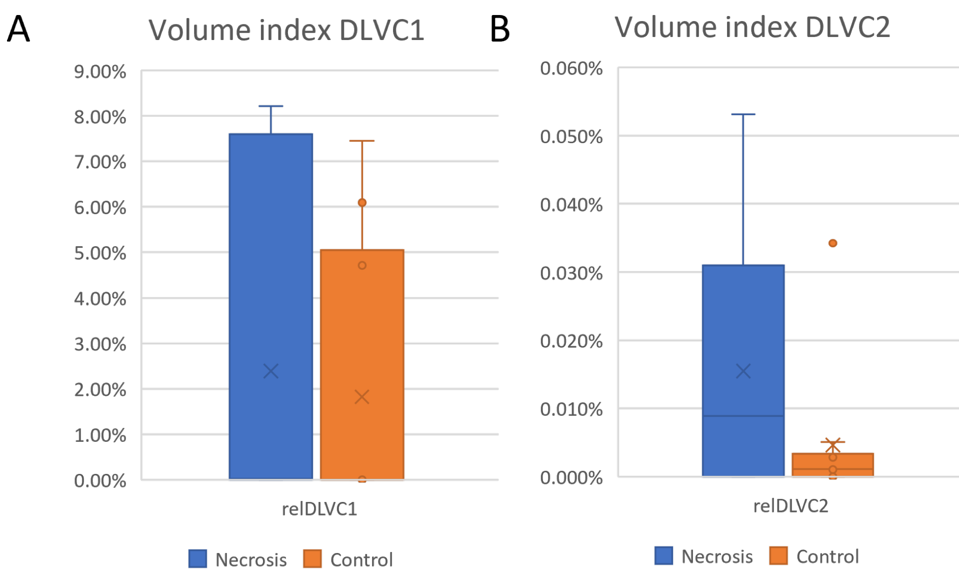

Figure 3.4: Comparison of DLVH index: *V(d,l)* between the AE and control patients at the two DLVCs.

CHAPTER 4
DISCUSSION

In this study, we tried to explore the correlation of BN with the joint distribution of dose and LET in CNS cancer patients treated with proton therapy. DLVHs were successfully derived from all the AE and control patients, and the *p*-value map was derived by comparing DLVHs between the AE group and control group using the Mann-Whitney U test. The typical DLVH indices, $V(d,l)$, were used to derive DLVCs that could be used to differentiate AE patients and control patients in the study.

Limitations of this study include a low number of patients studied, which makes discerning the real synergistic effect of LET and dose on RN occurrence more difficult due to the low signal to noise ratio in the data. For example, much of the left side of the "island" of Figure 3.2, which is shown to be statistically significantly different between the AE and control group ($p<0.05$), has high LET and low dose (<30Gy), implying that voxels with such dose and LET are likely to be involved in AE initialization. However, radiation necrosis is very unlikely to occur in areas receiving such low dose, indicating that this area of the *p*-value map may be artifacts rather than a valid area to derive DLVCs.

The low numbers of patients experiencing BN on one hand is a positive thing because the incidence rate of BN should be minimized as much as possible when planning radiation therapy, but also limits the amount of patient data, especially the number of AE patients, available to study these types of AEs. One possible method of increasing the study population would be to recruit from multiple cancer centers with PT, however this may introduce many more confounding factors such as inconsistencies between treatment planning software, radiation delivery equipment, and other institutional practices that may affect the way patients are treated using proton therapy among the different institutions.

Another limitation is the lack of spatial information in the DLVH plots. The DLVH method by itself aggregates all voxels in the selected contour to project into the 2D dose-LET plane; the spatial relationship between individual voxels is thus lost in the projection. In order to have a greater understanding of the interplay between the dose and LET delivered to patients and the likelihood of BN and other AEs, a more detailed examination of the spatial distribution of the affected voxels is needed, because each voxel does not exist its own space, but rather is interconnected with the other voxels surrounding it. Yang, et al (2022) [30] is an example of this idea to investigate the spatial relationship between different voxels with the AE region using seed-spot analysis, and this method could potentially be used in studying BN as well. The contours of the necrotic regions noted in the MRI, fused to the planning CT could be the starting point of such a study.

If more data on BN initiation could be collected in the future, it would be very desirable to create a normal tissue complication probability (NTCP) model based on the derived DLVCs, which could be used to create some dose and LET related optimization constraints that could be useful retrospectively in plan evaluation and prospectively in treatment planning to minimize the corresponding AEs. However, the limited number of patients included in this study prevents us from deriving a potential NTCP model.

The literature focusing on the effects of LET and dose on the RBE of protons has not reached a consensus yet. Some papers support the idea that LET is highly implicated in raising the RBE and thus should be factored into treatment planning workflows for PT patients; other studies have found the evidence for the LET effect in patient outcomes be equivocal. However, essentially all the investigators studying this topic agreed that RBE in proton therapy was a highly complex, multifactorial problem that is difficult to study *in vitro*. Experiments that rely on clonogenic cell survival data is unfortunately absent the effects of the immune system and tissue cell interactions that would be present in live test subjects, just as an example. Therefore, while this study does find evidence in support of the idea that high LET can increase BN incidence in CNS cancer patients treated with proton therapy, the conclusion is not definitive and requires much more study and experimentation before it can meaningfully inform future clinical practice for proton therapy.

CHAPTER 5

CONCLUSION

The aims of this study, to investigate potential ways to predict BN in patients undergoing CNS cancer patients undergoing proton therapy, was successful. The statistical comparison of dosimetric characteristics, i.e. DLVH, of CNS cancer patients who developed BN versus those who did not led to the introduction of DLVCs. The small number of available patient data limits the predictive power of the study and did not enable the formulation of a NTCP model specific to BN in CNS cancer patients treated with proton therapy. However, the data yielded from this study supports the hypothesis that the LET effect is significant in the AE initialization for cancer patients treated with proton therapy, and that proton plan evaluation and treatment planning should further incorporate LET as an input to minimize the possible incidence of unexpected AEs.

REFERENCES

[1] Song J, Aljabab S, Abduljabbar L, et al. Radiation-induced brain injury in patients with meningioma treated with proton or photon therapy. *J Neurooncol*. 2021;153(1):169-180. doi:10.1007/s11060-021-03758-y

[2] Chen YH, Molenaar D, Uyl-de Groot CA, Van Vulpen M, Blommestein HM. Medical Resource Use and Medical Costs for Radiotherapy-Related Adverse Effects: A Systematic Review. *Cancers*. 2022;14(10):2444. doi:10.3390/cancers14102444

[3] Vitti ET, Parsons JL. The Radiobiological Effects of Proton Beam Therapy: Impact on DNA Damage and Repair. *Cancers*. 2019; 11(7):946. https://doi.org/10.3390/cancers11070946

[4] Newhauser WD, Zhang R. The physics of proton therapy. *Phys Med Biol*. 2015;60(8):R155-R209. doi:10.1088/0031-9155/60/8/R155

[5] Paganetti H. Relative biological effectiveness (RBE) values for proton beam therapy. Variations as a function of biological endpoint, dose, and linear energy transfer. *Phys Med Biol*. 2014;59(22):R419-R472. doi:10.1088/0031-9155/59/22/R419

[6] Mohan R, Grosshans D. Proton therapy – Present and future. *Advanced Drug Delivery Reviews*. 2017;109:26-44. doi:10.1016/j.addr.2016.11.006

[7] Gaito S, Burnet N, Aznar M, et al. Normal Tissue Complication Probability Modelling for Toxicity Prediction and Patient Selection in Proton Beam Therapy to the Central Nervous System: A Literature Review. *Clinical Oncology*. 2022;34(6):e225-e237. doi:10.1016/j.clon.2021.12.015

[8] Indelicato DJ, Flampouri S, Rotondo RL, et al. Incidence and dosimetric parameters of pediatric brainstem toxicity following proton therapy. *Acta Oncologica*. 2014;53(10):1298-1304. doi:10.3109/0284186X.2014.957414

[9] Grosshans DR, Duman JG, Gaber MW, Sawakuchi G. Particle Radiation Induced Neurotoxicity in the Central Nervous System. *International Journal of Particle Therapy*. 2018;5(1):74-83. doi:10.14338/IJPT-18-00026.1

[10] Fossum CC, Beltran CJ, Whitaker TJ, Ma DJ, Foote RL. Biological Model for Predicting Toxicity in Head and Neck Cancer Patients Receiving Proton Therapy. *International Journal of Particle Therapy*. 2017;4(2):18-25. doi:10.14338/IJPT-17-00015

[11] Garbacz M, Cordoni FG, Durante M, et al. Study of relationship between dose, LET and the risk of brain necrosis after proton therapy for skull base tumors. *Radiotherapy and Oncology*. 2021;163:143-149. doi:10.1016/j.radonc.2021.08.015

[12] Niemierko A, Schuemann J, Niyazi M, et al. Brain Necrosis in Adult Patients After Proton Therapy: Is There Evidence for Dependency on Linear Energy Transfer? *International Journal of Radiation Oncology*Biology*Physics*. 2021;109(1):109-119. doi:10.1016/j.ijrobp.2020.08.058

[13] Bertolet A, Abolfath R, Carlson DJ, et al. Correlation of LET With MRI Changes in Brain and Potential Implications for Normal Tissue Complication Probability for Patients With Meningioma Treated With Pencil Beam Scanning Proton Therapy. *International Journal of Radiation Oncology*Biology*Physics*. 2022;112(1):237-246. doi:10.1016/j.ijrobp.2021.08.027

[14] Underwood TSA, McNamara AL, Appelt A, Haviland JS, Sørensen BS, Troost EGC. A systematic review of clinical studies on variable proton Relative Biological Effectiveness (RBE). *Radiotherapy and Oncology*. 2022;175:79-92. doi:10.1016/j.radonc.2022.08.014

[15] Paganetti H, Beltran C, Both S, et al. Roadmap: proton therapy physics and biology. *Phys Med Biol*. 2021;66(5):05RM01. doi:10.1088/1361-6560/abcd16

[16] Deng W, Yang Y, Liu C, et al. A Critical Review of LET-Based Intensity-Modulated Proton Therapy Plan Evaluation and Optimization for Head and Neck Cancer Management. *International Journal of Particle Therapy*. 2021;8(1):36-49. doi:10.14338/IJPT-20-00049.1

[17] Liu C, Patel SH, Shan J, et al. Robust Optimization for Intensity Modulated Proton Therapy to Redistribute High Linear Energy Transfer from Nearby Critical Organs to Tumors in Head and Neck Cancer. *International Journal of Radiation Oncology*Biology*Physics*. 2020;107(1):181-193. doi:10.1016/j.ijrobp.2020.01.013

[18] An Y, Shan J, Patel SH, et al. Robust intensity-modulated proton therapy to reduce high linear energy transfer in organs at risk. *Med Phys*. 2017;44(12):6138-6147. doi:10.1002/mp.12610

[19] Feng H, Shan J, Anderson JD, et al. Per-voxel constraints to minimize hot spots in linear energy transfer-guided robust optimization for base of skull head and neck cancer patients in IMPT. *Med Phys*. 2022;49(1):632-647. doi:10.1002/mp.15384

[20] Harrison N, Kang M, Liu R, et al. A Novel Inverse Algorithm To Solve the Integrated Optimization of Dose, Dose Rate, and Linear Energy Transfer of Proton FLASH Therapy With Sparse Filters. *International Journal of Radiation Oncology*Biology*Physics*. Published online December 2023:S0360301623081877. doi:10.1016/j.ijrobp.2023.11.061

[21] Liu R, Charyyev S, Wahl N, et al. An Integrated Physical Optimization Framework for Proton Stereotactic Body Radiation Therapy FLASH Treatment Planning Allows Dose, Dose Rate, and Linear Energy Transfer Optimization Using Patient-Specific Ridge Filters. *Int J Radiat Oncol Biol Phys*. 2023;116(4):949-959. doi:10.1016/j.ijrobp.2023.01.048

[22] Yang Y, Vargas CE, Bhangoo RS, et al. Exploratory Investigation of Dose-Linear Energy Transfer (LET) Volume Histogram (DLVH) for Adverse Events Study in Intensity Modulated Proton Therapy (IMPT). *International Journal of Radiation Oncology*Biology*Physics*. 2021;110(4):1189-1199. doi:10.1016/j.ijrobp.2021.02.024

[23] Deng W, Younkin JE, Souris K, et al. Technical Note: Integrating an open source Monte Carlo code "MCsquare" for clinical use in intensity-modulated proton therapy. *Med Phys*. 2020;47(6):2558-2574. doi:10.1002/mp.14125

[24] Deng W, Ding X, Younkin JE, et al. Hybrid 3D analytical linear energy transfer calculation algorithm based on precalculated data from Monte Carlo simulations. *Med Phys*. 2020;47(2):745-752. doi:10.1002/mp.13934

[25] Holmes J, Shen J, Shan J, et al. Technical note: Evaluation and second check of a commercial Monte Carlo dose engine for small-field apertures in pencil beam scanning proton therapy. *Med Phys*. 2022;49(5):3497-3506. doi:10.1002/mp.15604

[26] Shan J, Feng H, Morales DH, et al. Virtual particle Monte Carlo: A new concept to avoid simulating secondary particles in proton therapy dose calculation. *Med Phys*. 2022;49(10):6666-6683. doi:10.1002/mp.15913

[27] Feng H, Holmes JM, Vora SA, et al. Modelling small block aperture in an in-house developed GPU-accelerated Monte Carlo-based dose engine for pencil beam scanning proton therapy. *Phys Med Biol*. 2024;69(3):10.1088/1361-6560/ad0b64. Published 2024 Jan 17. doi:10.1088/1361-6560/ad0b64

[28] Yang Y, Rwigema JM, Vargas C, et al. Technical note: Investigation of dose and LETd effect to rectum and bladder by using non-straight laterals in prostate cancer receiving proton therapy. *Med Phys*. 2022;49(12):7428-7437. doi:10.1002/mp.16008

[29] Yang Y, Muller OM, Shiraishi S, et al. Empirical Relative Biological Effectiveness (RBE) for Mandible Osteoradionecrosis (ORN) in Head and Neck Cancer Patients Treated With Pencil-Beam-Scanning Proton Therapy (PBSPT): A Retrospective, Case-Matched Cohort Study. *Front Oncol*. 2022;12:843175. doi:10.3389/fonc.2022.843175

[30] Yang Y, Patel SH, Bridhikitti J, et al. Exploratory study of seed spots analysis to characterize dose and linear-energy-transfer effect in adverse event initialization of pencil-

beam-scanning proton therapy. *Medical Physics*. Published online July 21, 2022:mp.15859. doi:10.1002/mp.15859

[31] Lin LI. A concordance correlation coefficient to evaluate reproducibility. Biometrics. 1989;45(1):255-268.

[32] Wang Y, Holland SK, Vannest J. Concordance of MEG and fMRI patterns in adolescents during verb generation. *Brain Res*. 2012;1447:79-90. doi:10.1016/j.brainres.2012.02.001